Viral delivery of tissue nonspecific alkaline phosphatase diminishes craniosynostosis in one of two FGFR2$^{C342Y/+}$ mouse models of Crouzon syndrome.

Hwa Kyung Nam[1], Iva Vesela[1], Sara Dean Schutte[1], Nan E. Hatch[1*]

[1] Department of Orthodontics and Pediatric Dentistry, School of Dentistry, University of Michigan, Ann Arbor, Michigan, United States of America

* Corresponding author
E-mail: nhatch@umich.edu

Abstract

Craniosynostosis is the premature fusion of cranial bones. The goal of this study was to determine if delivery of recombinant tissue nonspecific alkaline phosphatase (TNAP) could prevent or diminish the severity of craniosynostosis in a C57BL/6 FGFR2$^{C342Y/+}$ model of neonatal onset craniosynostosis or a BALB/c FGFR2$^{C342Y/+}$ model of postnatal onset craniosynostosis. Mice were injected with a lentivirus encoding a mineral targeted form of TNAP immediately after birth. Cranial bone fusion as well as cranial bone volume, mineral content and density were assessed by micro computed tomography. Craniofacial shape was measured with calipers. Alkaline phosphatase, alanine amino transferase (ALT) and aspartate amino transferase (AST) activity levels were measured in serum. Neonatal delivery of TNAP diminished craniosynostosis severity from 94% suture obliteration in vehicle treated mice to 67% suture obliteration in treated mice, $p<0.02$) and the incidence of malocclusion from 82.4% to 34.7% ($p<0.03$), with no effect on cranial bone in C57BL/6 FGFR2$^{C342Y/+}$ mice. In contrast, treatment with TNAP improved cranial bone volume ($p< 0.01$), density ($p< 0.01$) and mineral content ($p< 0.01$) but had no effect on craniosynostosis or malocclusion in BALB/c FGFR2$^{C342Y/+}$ mice. These results indicate that perinatal recombinant TNAP enzyme therapy diminishes craniosynostosis severity in the C57BL/6 FGFR2$^{C342Y/+}$ neonatal onset mouse model of Crouzon syndrome, and that effects of exogenous TNAP are genetic background dependent.

41 # Introduction

42 Skull growth occurs via intramembranous bone deposition along the outer edge of each
43 cranial vault bone, in coordination with endochondral growth of cranial base bones at the
44 cranial base synchondroses (cartilaginous growth plates). Anterior-posterior growth of the skull
45 is dependent upon both cranial vault and cranial base bone growth. Craniosynostosis (which,
46 when syndromic also often includes premature fusion of cranial base bones) can lead to high
47 intracranial pressure, abnormal skull and facial shapes, malocclusion, blindness, seizures and
48 brain abnormalities [1-6]. Because the sole treatment is surgery, even with appropriately early
49 diagnosis patients can suffer high morbidity [7-9]. A pharmaceutical treatment for
50 craniosynostosis is not yet realized.

51 Activating mutations in Fibroblast Growth Factor Receptor 2 (*Fgfr2)* [10-13] and inactivating
52 mutations in *Alpl*, the gene for tissue nonspecific alkaline phosphatase (TNAP) [14-17] can cause
53 craniosynostosis. In this study we sought to determine if treatment with recombinant mineral-
54 targeted TNAP could rescue craniosynostosis and associated craniofacial skeletal abnormalities
55 in the FGFR2$^{C342Y/+}$ Crouzon mouse model of craniosynostosis, when delivered shortly post-natal
56 with lentivirus. The FGFR2$^{C342Y/+}$ mutation was previously demonstrated to cause ligand
57 independent signaling and is therefore widely considered to be an activating mutation leading
58 to increased FGF signaling [18-21]. We pursued this investigation because we previously
59 demonstrated that FGF signaling diminishes TNAP expression [22-24], and showed that TNAP
60 deficiency in mice leads to a similar craniofacial phenotype to that seen in FGFR2$^{C342Y/+}$ Crouzon
61 mice including coronal but not sagittal craniosynostosis, deficient growth of the cranial base
62 with fusion of cranial base synchondroses, and brachycephalic/acrocephalic (wide/tall) head

shapes [11, 17, 25, 26]. Additionally, in a previous study using archival aliquots of lentivirus expressing the mineral targeted recombinant form of TNAP that resulted in increases in serum AP activity in only a small number of the treated mice, we found statistical differences in the morphology of the inferior skull surface in treated vs. untreated BALB/c FGFR2$^{C342Y/+}$ mice [27].

Craniosynostosis onset in humans can occur pre-, peri- or postnatal, with earlier onset forms leading to more severe outcomes and higher morbidity. We backcrossed FGFR2$^{C342Y/+}$ mice onto C57BL/6 and BALB/c strains, and found that C57BL/6 FGFR2$^{C342Y/+}$ mice exhibit obliteration of the coronal cranial suture initiating shortly after birth, while BALB/c FGFR2$^{C342Y/+}$ mice exhibit point fusions across the coronal suture initiating at four weeks after birth [25]. Both FGFR2$^{C342Y/+}$ strains of mice also exhibit deficient cranial base growth with brachycephalic/acrocephalic head shapes and tendency for a class III malocclusion (lower teeth protruding anterior to upper teeth). The objective of this study was to determine if postnatal delivery of recombinant TNAP could diminish the severity of craniosynostosis in FGFR2$^{C342Y/+}$ mice, a model of Crouzon craniosynostosis syndrome. Viral delivery of TNAP was tested in both C57BL/6 FGFR2$^{C342Y/+}$ and BALB/c FGFR2$^{C342Y/+}$ mice to determine if efficacy is dependent upon timing of craniosynostosis onset and/or severity of fusion.

Materials and methods

TNAP Lentivirus

Recombinant mineral-targeted TNAP lentivirus was generously provided by Dr. Jose Luis Millán (Sanford Burnham Prebys Medical Discovery Institute, La Jolla, CA). Pseudotype of the virus is VSV-G, for transduction into multiple cell types. The SJ1-based HIV-1 vector contains 0.25 kB

85 insulators derived from the chicken beta-globin locus to diminish insertional mutagenesis,
86 increase viral titer and increase protein expression [28]. The virus expresses a mineral-targeted
87 protein that is composed of soluble human TNAP enzyme fused to the constant region of
88 human IgG1 and a C-terminal deca-aspartate motif to confer targeting to hydroxyapatite. The
89 aspartate tag confers 30x higher affinity for hydroxyapatite than untagged enzyme [29].
90 Longevity of the virus for increasing AP levels was reported to last at least 60 days when
91 injected into neonatal mice and biodistribution of the virus was previously reported to be high
92 in the liver [30]. Treatment with this recombinant form of TNAP was previously shown to
93 increase serum alkaline phosphatase levels and rescue bone defects seen in hypophosphatasia
94 [14, 30-33]. Production and titer of the lentivirus for this study was performed by the University
95 of Michigan Vector Core.
96

97 Animal Procedures

98 Because severity of craniosynostosis and associated craniofacial shape defects are variable on
99 the mixed genetic background, FGFR2$^{C342Y/+}$mice were backcrossed with BALB/c and C57BL/6
100 mice (obtained from Charles River Laboratories) for at least fifteen generations prior to
101 experiments. BALB/c FGFR2$^{C342Y/+}$mice have a more moderate form of Crouzon syndrome with
102 craniosynostosis in the form of point fusions across the coronal suture first apparent between
103 three and four weeks after birth [25]. C57BL/6 mice have a more severe form of Crouzon
104 syndrome with craniosynostosis in the form of suture obliteration first apparent in neonatal mice
105 (**Fig. 1**). Both mice also exhibit abnormalities in the cranial base and deficient cranial base growth.

106 Genotyping was performed as previously described [11, 25]. Briefly, DNA from tail digests was
107 amplified by polymerase chain reaction using 5'-gagtaccatgctgactgcatgc-3'and 5'-
108 ggagaggcatctctgtttcaagacc-3' primers to yield a 200 base pair band for wild type FGFR2 and a 300
109 base pair band for mutant $FGFR2^{C342Y}$. Mice were fed ad libitum and housed under standard 12
110 hour dark/light cycles. Litters were randomly assigned to treatment/no treatment groups.
111 Treated mice were injected with 1.0 x 10^7 transforming units lentivirus or an equivalent volume
112 of phosphate buffered saline via the jugular vein after birth. BALB/c mice (n=12 $FGFR2^{+/+}$ vehicle
113 treated mice, n=14 $FGFR2^{C342Y/+}$ vehicle treated mice, n=16 $FGFR2^{C342Y/+}$ TNAP lentivirus treated
114 mice) were euthanized by CO_2 overdose at four weeks post-natal and C57BL/6 mice (n=14
115 $FGFR2^{+/+}$ vehicle treated mice, n=14 $FGFR2^{C342Y/+}$ vehicle treated mice, n=17 $FGFR2^{C342Y/+}$ TNAP
116 lentivirus treated mice) were euthanized by CO_2 overdose at three weeks post-natal for analyses.
117 BALB/c mice were sacrificed at a later age than C57BL/6 mice because craniosynostosis onset
118 occurs later in BALB/C than in C57BL/6 $FGFR2^{C342Y/+}$ mice. Blood was collected by aortic puncture
119 under surgical anesthesia. Mice were weighed, and body length was measured for each animal.
120 All animal procedures were prospectively approved of by the University of Michigan's University
121 Committee on Use and Care of Animals (UCUCA, protocol PRO00006815). All samples were de-
122 identified as to genotype and treatment group for analyses, then unblinded for statistical
123 comparison. The primary outcome assessment was craniosynostosis incidence. Secondary
124 outcome assessments included malocclusion incidence, cranial bone micro CT measurements,
125 craniofacial shape measurements, and cranial base bone lengths.

126

127 **Serum Analyses**

128 Mice were fasted for six hours prior to blood collection. Alkaline phosphatase activity (AP) in
129 serum was quantified using the colorimetric reagent 4-nitrophenyl-phosphate disodium
130 hexahydrate (Sigma-Aldrich), as compared to a standard curve using commercially available
131 alkaline phosphatase enzyme (Sigma-Aldrich). One unit of AP was defined as the amount of
132 enzyme needed to generate 1 umol of p-nitrophenol per minute. Inorganic phosphate
133 quantifications were performed using commercially available kits (Pointe Scientific), also as
134 compared to standard curves. The levels of alanine amino transferase (ALT) and Aspartate
135 amino transferase (AST) were determined using commercially available colorimetric assay kits
136 according to manufacturer instructions (Sigma-Aldrich) using serum from control and treated
137 BALB/c mice, as these mice yielded more serum per mouse. One unit of ALT was defined as the
138 as the amount of enzyme that would generate 1 nmol of pyruvate per minute. One unit of AST
139 was defined as the amount of enzyme that would generate 1 nmol of glutamate per minute.
140

141 **Micro Computed Tomography**

142 Whole skulls were scanned at an 18 µm isotropic voxel resolution using the eXplore Locus SP
143 micro computed tomography imaging system (GE Healthcare Pre-Clinical Imaging, London, ON,
144 Canada). Regions of interest (ROI's) for parietal and frontal bones were established as 0.5 mm
145 in length, 0.5 mm in width, and depth equivalent to thickness of bone, as previously described
146 [17, 25]. Density, volume and mineral content of cranial bones from mice were measured using
147 previously established methods using Microview version 2.2 software (GE Healthcare Pre-
148 Clinical Imaging, London, ON) and established algorithms [34, 35]. Linear measurements of

149 cranial base bones were measured on micro CT scans using Dolphin imaging software (Dolphin
150 Imaging & Management Solutions).
151

152 Cranial Suture and Cranial Base Synchondrosis Assessment

153 Fusions between frontal and parietal cranial bones (fusion of the coronal suture), fusion between
154 parietal bones (fusion of the sagittal suture) and fusion of the intersphenoidal synchondrosis (ISS)
155 and spheno-occipital synchondrosis (SOS) were identified on micro CT scans of mouse skulls.
156 Cranial sutures and synchondroses were viewed using the two-dimensional micro CT slices in an
157 orthogonal view across the entire length of the suture or synchondrosis, as previously described
158 [17, 25]. Synchondroses were identified as fused or not fused. To distinguish between more vs.
159 less severe forms of craniosynostosis, fusion of cranial suture was scored in the following
160 categories: 0) normal open suture, 1) diminished suture width with no fusion 2) diminished
161 suture width with point fusions, and 3) obliteration of the suture.
162 Reliability of suture fusion assessment was verified by both intra-operator and inter-
163 operator reliability statistics by calculating intraclass correlation coefficients (ICC). Intra-
164 operator reliability statistics was carried out by assessing suture fusion status of the coronal
165 and sagittal sutures as well as the ISS and SOS synchondroses on fifteen micro CT scans by one
166 investigator two times separated by a two-month period. Inter-operator reliability was carried
167 out by analyzing fifteen micro CT scans by a second investigator. The ICC for intraoperator
168 reliability for fusion assessment is .970 ($p \leq .0001$) and the ICC for interoperator reliability is .972
169 ($p \leq .0001$). Thus, there is high intraoperator and interoperator reliability for fusion assessment.

170

171 ## Linear Measurements

172 Craniofacial linear skeletal measurements were taken using digital calipers on dissected skulls.
173 Linear measurements were calculated using previously reported craniofacial skeletal landmarks
174 [25, 36, 37], including standard measurements currently in use by the Craniofacial Mutant Mouse
175 Resource of Jackson Laboratory (Bar Harbor, ME). Linear measurements were normalized to total
176 skull length (measured from nasale to opisthion) to account for size differences between
177 $FGFR2^{+/+}$ and $FGFR2^{C342Y/+}$ mice. Measurements were performed twice and an average of the two
178 measurements was utilized for statistical comparison by genotype and treatment. Cranial base
179 anterior-posterior bone lengths were measured on micro CT scans using *Dolphin Imaging 11.0*
180 software (Dolphin Imaging and Management Solutions, Chatsworth, CA), as previously described
181 [26].

182

183 ## Statistics

184 Results from previous studies and this study demonstrate no sex difference for craniosynostosis
185 in $FGFR2^{C342Y/+}$ mice, therefore sexes were combined for analyses [25]. Normality of data was
186 evaluated by D'Agostino & Pearson Tests. Students t test was then used to compare groups of
187 that were of normal distribution and the Mann Whitney test was utilized to compare groups of
188 that were of non-normal distribution. Because serum AP levels varied in mice injected with the
189 lentivirus, linear regressions were performed to determine if, and to what extent serum AP
190 levels associated with changes body weight and serum liver enzyme levels. Incidences of

craniosynostosis severity category, synchondrosis fusion and malocclusion were analyzed by the Fisher's exact test.

Results

Injection with the TNAP expression lentivirus significantly increased serum AP levels in all of the treated mice (**Table 1**). BALB/c FGFR2$^{C342Y/+}$ mice injected with the lentivirus increased serum AP levels by 1.2 U/mL when compared to BALB/c vehicle treated FGFR2$^{C342Y/+}$ mice ($p<0.0001$) when measured at four weeks old. C57BL/6 FGFR2$^{C342Y/+}$ mice injected with the TNAP expression lentivirus increased serum AP levels by 1.8 U/mL when compared to vehicle treated C57BL/6 FGFR2$^{C342Y/+}$ mice ($p<0.0001$) when measured at three weeks old. No significant difference in serum AP levels were seen between untreated FGFR2$^{C342Y/+}$ and FGFR2$^{+/+}$ mice on the BALB/c or C57BL/6 backgrounds. Injection with the lentivirus did not alter serum inorganic phosphate (P_i) levels.

Table 1. Serum Alkaline Phosphatase and Inorganic Phosphate Measurements in vehicle vs. TNAP treated BALB/c and C57Bl/6 mice.

Strain	Genotype	Treatment	Serum AP Level (units/ml)	Serum Pi Level (mg/dl)
BALB/c	FGFR2$^{+/+}$	vehicle	0.03 +/- 0.01	10.9 +/- 0.8
BALB/c	FGFR2$^{C342Y/+}$	vehicle	0.03 +/- 0.78	9.9 +/- 1.4
BALB/c	FGFR2$^{C342Y/+}$	TNAP	1.30 +/- 0.54$^{\#}$	9.8 +/- 1.1
C57Bl/6	FGFR2$^{+/+}$	vehicle	0.01 +/- 0.01	9.5 +/- 1.0
C57Bl/6	FGFR2$^{C342Y/+}$	vehicle	0.02 +/- 0.01	8.7 +/- 1.1
C57Bl/6	FGFR2$^{C342Y/+}$	TNAP	1.93 +/- 0.77$^{\#}$	9.0 +/- 0.6

$^{\#}$ p value < 0.01 between treatment groups

224 Statistical comparison of groups by Mann Whitney showed that FGFR2$^{C342Y/+}$ mice weigh less
225 and are shorter in body length than their wild type littermates, regardless of genetic
226 background (**Fig. 2**). Qualitative analysis of craniofacial skeletal shape suggested that
227 FGFR2$^{C342Y/+}$ mice differ in morphology from their wild type counterparts, and that delivery of
228 mineral-targeted TNAP via lentivirus did not impact skull morphology (**Fig. 3**).
229 Craniofacial skeletal linear measurements normalized to total skull length revealed many
230 differences between FGFR2$^{342Y/+}$ and FGFR2$^{+/+}$ mice on both congenic backgrounds (**Table 2**).

231 **Table 2.** Linear Craniofacial Skeletal Measurements reveals
232 no rescue of craniofacial shape in by TNAP treatment in FGFR2$^{C342Y/+}$ mice.

Strain	Measurement	FGFR2$^{+/+}$ vehicle	FGFR2$^{C342Y/+}$ vehicle	FGFR2$^{C342Y/+}$ TNAP
BALB/c	Cranial Height	.36 +/- .01*	.45 +/- .01	.45 +/- .01
BALB/c	Cranial Width	.55 +/- .01*	.63 +/- .01	.62 +/- .01
BALB/c	Inner Canthal Distance	.20 +/- .01*	.25 +/- .01	.26 +/- .01
BALB/c	Nose Length	.65+/- .01	.65 +/- .01	.65 +/- .01
BALB/c	Nasal Bone Length	.33 +/- .02*	.32 +/- .01	.32 +/- .03
BALB/c	Frontal Bone length	.33 +/- .02	.33 +/- .01	.34 +/- .03
BALB/c	Parietal Bone Length	.20 +/- .01*	.25 +/- .02	.26 +/- .01
BALB/c	Ratio Height to Width	.66 +/- .02*	.72 +/- .02	.72 +/- .02
C57Bl/6	Cranial Height	.38 +/- .01*	.52 +/- .01	.52 +/- .03
C57Bl/6	Cranial Width	.55 +/- .01*	.64 +/- .01	.64 +/- .02
C57Bl/6	Inner Canthal Distance	.23 +/- .01*	.29 +/- .01	.29 +/- .01
C57Bl/6	Nose Length	.65 +/- .01*	.62 +/- .01	.63 +/- .03
C57Bl/6	Nasal Bone Length	.32 +/- .01*	.23 +/- .02	.23 +/- .01
C57Bl/6	Frontal Bone length	.35 +/- .01*	.40 +/- .02	.41 +/- .03
C57Bl/6	Parietal Bone Length	.22 +/- .01*	.26 +/- .02	.27 +/- .02
C57Bl/6	Ratio Height to Width	.38 +/- .01*	.52 +/- .01	.52 +/- .03

233
234 Measures are reported as normalized to total skull length.
235 * p value < 0.01 between genotypes
236 No statistical differences between treatment groups were found.
237

238 BALB/c FGFR2$^{C342Y/+}$ mice had increased cranial height, cranial width, inner canthal distance,
239 parietal bone length and cranial height to width ratios, with decreased nasal bone length.
240 C57BL/6 FGFR2$^{C342Y/+}$ mice had increased cranial height, cranial width, inner canthal distance,
241 frontal bone length, parietal bone length and cranial height to width ratios, with decreased
242 nose and nasal bone lengths. Treatment with the TNAP lentivirus did not alter craniofacial
243 skeletal measurements in FGFR2$^{C342Y/+}$ mice on either genetic background.
244 Analysis of coronal suture fusions revealed diminished suture width (grade 1) in the
245 majority of BALB/c FGFR2$^{C342Y/+}$ vehicle treated mice with point fusions (grade 2) evident in
246 approximately 30% of the mice. In the more severe C57BL/6 FGFR2$^{C342Y/+}$ vehicle treated mice,
247 the majority of the mice had obliteration of the suture (grade 3) with point fusions (grade 2)
248 evident in the rest of the mice (**Fig. 4**). The sagittal suture was not fused in any of the mice, and
249 no cranial suture fusions were evident in wild type mice on either background. Treatment with
250 recombinant TNAP had no significant impact on the incidence of grade 1, 2 or 3 of the coronal
251 suture in the BALB/c FGFR2$^{C342Y/+}$ mice. While there was only a trend for decreased fusion in the
252 left coronal suture fusion upon treatment (control 94% suture obliteration vs. treated 78%
253 suture obliteration), there was a significant decrease in coronal suture fusion upon treatment in
254 the right coronal suture (control 94% suture obliteration vs. treated 57% suture obliteration,
255 $p<0.03$). There was also a significant decrease in coronal suture fusion when combining both
256 right and left coronal sutures (control 94% suture obliteration vs. treated 67% suture
257 obliteration, $p<0.02$). Consistent with rescue of coronal suture fusion in C57BL/6 but not BALB/c
258 mice, the incidence of malocclusion was also significantly decreased by treatment from 82.4%
259 to 34.7% in C57BL/6 but not BALB/c FGFR2$^{C342Y/+}$ mice (**Fig. 5**, $p<0.03$).

260 Analysis of cranial base synchondrosis fusions revealed a 100% incidence of fusion of the
261 inter-sphenoidal synchondrosis (ISS) in both strains of FGFR2$^{C342Y/+}$ mice, with no fusions
262 evident in wild type mice. Comparison of vehicle vs. treated mice revealed no significant change
263 in the incidence of ISS fusion in FGFR2$^{C342Y/+}$ mice on either genetic background. Spheno-
264 occipital synchondronsis (SOS) fusion was seen in approximately half of C57BL/6 FGFR2$^{C342Y/+}$
265 mice but rarely in BALB/c FGFR2$^{C342Y/+}$ mice. Comparison of vehicle vs. treated mice revealed no
266 significant change in the incidence of SOS fusion in FGFR2$^{C342Y/+}$ mice on either genetic
267 background. Measurements of cranial base bone lengths demonstrated decreased length of the
268 basis-sphenoid and pre-sphenoid bones in both BALB/c and C57BL/6 vehicle treated
269 FGFR2$^{C342Y/+}$ as compared to FGFR2$^{+/+}$ mice (**Table 3**). Treatment increased length of the pre-
270 sphenoid bone in BALB/c and C57BL/6 FGFR2$^{C342Y/+}$ mice, but not to the equivalent of pre-
271 sphenoid bone length seen in FGFR2$^{+/+}$ mice.

272 **Table 3.** Cranial Base Bone Measurements in vehicle vs.
273 TNAP treated Balb/C and C57Bl/6 mice.
274
275
276
277

Strain	Genotype	Treatment	Basis Occipitus (mm)	Basis Sphenoid (mm)	Pre-Sphenoid (mm)
Balb/C	FGFR2$^{+/+}$	vehicle	3.1 +/- 0.1	2.9 +/- 0.1*	2.5 +/- 0.1*
Balb/C	FGFR2$^{C342Y/+}$	vehicle	2.9 +/- 0.3	2.4 +/- 0.3	1.8 +/- 0.1
Balb/C	FGFR2$^{C342Y/+}$	TNAP	2.9 +/- 0.2	2.5 +/- 0.3	1.9 +/- 0.1$^{\#}$
C57Bl/6	FGFR2$^{+/+}$	vehicle	2.8 +/- 0.2	2.9 +/- 0.2*	2.2 +/- 0.1*
C57Bl/6	FGFR2$^{C342Y/+}$	vehicle	2.8 +/- 0.1	2.7 +/- 0.1	1.7 +/- 0.1
C57Bl/6	FGFR2$^{C342Y/+}$	TNAP	3.0 +/- 0.2	2.6 +/-0.1	1.9 +/- 0.1$^{\#}$

278
279
280
281
282
283
284
285
286
287
288
289
290 * p value < 0.01 between genotypes
291 No significant differences between treatment groups were found.
292
293 Micro CT based analyses of cranial bones demonstrated significantly diminished bone

294 mineral density, tissue mineral content, tissue mineral density and bone volume fraction in

295 frontal bones, plus significantly diminished tissue mineral density and bone volume fraction in

296 parietal bones of vehicle treated FGFR2$^{C342Y/+}$ mice when compared to wild type littermates on

297 both BALB/c and C57BL/6 backgrounds (**Table 4**). Injection with the TNAP lentivirus

298 significantly increased frontal bone mineral density, tissue mineral content and bone volume

299 fraction, plus parietal bone volume fraction in FGFR2$^{C342Y/+}$ mice on the BALB/c background.

300 Injection with the TNAP lentivirus did not significantly impact any of the cranial bone

301 parameters in FGFR2$^{C342Y/+}$ mice on the C57BL/6 background.

302 **Table 4.** Cranial bone volume, density and mineral content
303 in vehicle vs. TNAP treated BALB/c and C57BL/6 mice.

Strain	Genotype	Treatment	Cranial Bone	Bone Mineral Content (mg)	Bone Mineral Density (mg/cc)	Tissue Mineral Content (mg)	Tissue Mineral Density (mg/cc)	Bone Volume Fraction
BALB/c	FGFR2$^{+/+}$	vehicle	Frontal	.035 +/- .004	405 +/- 14*	.028 +/- .007*	692 +/- 14*	0.41 +/- .03*
BALB/c	FGFR2$^{C342Y/+}$	vehicle	Frontal	.031 +/- .008	361 +/- 63	.020 +/- .006#\	671 +/- 18	0.36 +/- .0
BALB/c	FGFR2$^{C342Y/+}$	TNAP	Frontal	.035 +/- .005	401 +/- 26#	.026 +/- .015#	683 +/- 29	0.42 +/- .06#
BALB/c	FGFR2$^{+/+}$	vehicle	Parietal	.034 +/- .004	405 +/- 12	.023 +/- .005	693 +/- 15*	0.43 +/- .03*
BALB/c	FGFR2$^{C342Y/+}$	vehicle	Parietal	.031 +/- .007	396 +/- 39	.020 +/- .005	669 +/- 24	0.36 +/- .06
BALB/c	FGFR2$^{C342Y/+}$	TNAP	Parietal	.034 +/- .006	403 +/- 27	.025 +/- .012	691 +/- 36	0.42 +/- .07#
C57BL/6	FGFR2$^{+/+}$	vehicle	Frontal	.017 +/- .003	245 +/- 25*	.006 +/- .001*	570 +/- 18*	0.12 +/- .01*
C57BL/6	FGFR2$^{C342Y/+}$	vehicle	Frontal	.013 +/- .002	209 +/- 25	.004 +/- .001	519 +/- 26	0.10 +/- .01
C57BL/6	FGFR2$^{C342Y/+}$	TNAP	Frontal	.016 +/- .004	225 +/- 30	.004 +/- .001	553 +/- 40	0.11 +/- .01
C57BL/6	FGFR2$^{+/+}$	vehicle	Parietal	.015 +/- .001	237 +/- 19	.005 +/- .001	590 +/- 13*	.121 +/- .023*
C57BL/6	FGFR2$^{C342Y/+}$	vehicle	Parietal	.012 +/- .003	217 +/- 18	.004 +/- .001	558 +/- 36	.098 +/- .006
C57BL/6	FGFR2$^{C342Y/+}$	TNAP	Parietal	.013 +/- .004	232 +/- 42	.004 +/- .001	575 +/- 32	.105 +/- .009

304
305 * p value < 0.01 between genotypes
306 # p value < 0.01 between treatment groups

307 Biodistribution of lentivirus containing the recombinant mineral-targeted form of TNAP was
308 previously shown to result in highest viral expression levels in the liver [30]. Because the
309 treated mice in this study received recombinant TNAP via lentivirus, while the control group
310 received no virus, we measured serum liver enzymes levels to determine if liver toxicity due to
311 lentivirus could account for a change in phenotype in the treated mice, and/or the increase in
312 serum AP levels seen in the treated mice. Alanine amino transferase (ALT) and Aspartate amino
313 transferase (AST) are liver enzymes that, when seen at high levels in serum, are indicative of
314 liver toxicity [38, 39]. Therefore, we tested serum ALT and AST levels in the mice. When
315 compared by genotypes, no differences were noted between $FGFR2^{+/+}$ and control $FGFR2^{C342Y/+}$
316 mice for either ALT or AST enzymes. When compared by treatment groups, $FGFR2^{C342Y/+}$ mice
317 that were treated had significantly lower ALT levels than their control counterparts, and
318 significantly higher levels of ALT than their control counterparts (**Fig. 6**). We next performed
319 correlation studies between ALT and AST serum levels with serum AP levels and body weight to
320 better understand if lentiviral delivery of TNAP led to liver toxicity. No significant correlations
321 were found between serum AP and AST levels for any of the groups. A significant reverse
322 correlation was found between serum AP and ALT levels only for the treated $FGFR2^{C342Y/+}$ group
323 ($r = -.73$; 95% confidence interval of -.898 to -.361, $p < .005$). No significant correlations were
324 found between serum AST or ALT levels and body weight for any of the groups. Together, this
325 data shows that the effect of lentiviral TNAP treatment decreased ALT and increased AST
326 enzymes in serum, but had no effect on body weight of the mice and was not likely causal for
327 the observed increased in serum AP levels seen in treated mice.

328

329 # Discussion

330 Here we found that neonatal lentiviral delivery of recombinant TNAP improved cranial bone
331 density, mineral content and volume fraction in the milder BALB/c FGFR2$^{C342Y/+}$ model of
332 Crouzon syndrome but not in the more severe C57BL/6 FGFR2$^{C342Y/+}$ model of Crouzon
333 syndrome. Improvement of cranial bone density, mineral content and volume fraction by TNAP
334 treatment in BALB/c Crouzon mice is consistent with results showing that recombinant mineral
335 targeted TNAP treatment rescues mineralization of craniofacial and long bones in in the *Alpl*$^{-/-}$
336 mouse model of infantile hypophosphatasia (HPP) and humans with infantile and childhood
337 HPP [30, 31, 33, 40]. It is curious that delivery of mineral-targeted TNAP did not improve cranial
338 bone parameters in the more severe C57BL/6 FGFR2$^{C342Y/+}$ mice. Wild type C57BL/6 mice have
339 significantly less cranial bone density, mineral content and volume fraction than BALB/c wild
340 type mice, which is diminished to an even greater extent in FGFR2$^{C342Y/+}$ C57BL/6 mice. While
341 not quantified here, it is possible that the lack of rescue by TNAP is due to diminished bone
342 matrix available to mineralize and/or a lack of cranial bone progenitor cells available to
343 generate additional bone in the C57BL/6 mice, as TNAP is known to be essential for matrix
344 mineralization [41] and for the formation of cranial bone progenitor cells [42].

345 Craniosynostosis severity was significantly diminished by treatment in the C57BL/6
346 FGFR2$^{C342Y/+}$ mice. The vast majority of these mice typically exhibit obliteration of the coronal
347 suture within a few days after birth (**Fig. 1**). Suture obliteration went from 94% to 67% in the
348 C57BL/6 FGFR2$^{C342Y/+}$ mice upon treatment with exogenous TNAP by three weeks after birth.
349 This result is consistent with the rescue of craniosynostosis seen in *Alpl*$^{-/-}$ mice treated with
350 mineral targeted recombinant TNAP protein [33]. While far from a complete rescue, the data

351 provided here does demonstrate the potential efficacy of TNAP for diminishing severity of
352 craniosynostosis in Crouzon syndrome. The data also supports the idea that convergence exists
353 between changes downstream of TNAP activity and FGFR2 signaling leading to coronal suture
354 fusion. We recently showed that TNAP regulates expression of FGFR2 and Erk1,2 activity [42].
355 While the current study was originally based upon the hypothesis that FGF signaling regulates
356 expression of TNAP, our more recent data suggests the alternative hypothesis that exogenous
357 delivery of TNAP rescues Crouzon craniosynostosis because TNAP diminishes the overactive FGF
358 and Erk1,2 signaling in FGFR2$^{C342Y/+}$ cells. We are currently working to confirm this latter
359 hypothesis and delineate how TNAP may mediate these changes.
360 This study was designed to include two mouse models of Crouzon syndrome: a severe form
361 (C57BL/6 FGFR2$^{C342Y/+}$ mice) that exhibited neonatal onset of coronal suture obliteration and a
362 more moderate form (BALB/c FGFR2$^{C342Y/+}$ mice) that exhibited small point fusions across the
363 coronal suture evident by four weeks after birth. We anticipated that neonatal delivery of TNAP
364 via lentivirus would have greater effects on the later onset BALB/c FGFR2$^{C342Y/+}$ mouse model,
365 as the drug would be delivered prior to onset of craniosynostosis. Results showed instead that
366 the treatment significantly diminished severity of coronal suture fusion in the neonatal onset
367 C5BL/6 FGFR2$^{C342Y/+}$ mouse with no effect on coronal suture fusion in the postnatal onset
368 BALB/c FGFR2$^{C342Y/+}$ mouse. This data suggests that exogenous TNAP may be able to prevent
369 cranial suture obliteration but not point fusions across the suture. This data also indicates that
370 cellular mechanisms leading to craniosynostosis in FGFR2$^{C342Y/+}$ mice are both independent and
371 dependent upon TNAP.

372 While lentiviral TNAP treatment did not rescue cranial base synchondrosis fusion in the
373 FGFR2$^{C342Y/+}$ mice, length of the pre-sphenoid bone was mildly increased in the treated mice.
374 This result is consistent with our previous study using archival lots of the lentivirus [27] which
375 suggested changes in inferior skull morphology and may indicate that TNAP can promote cranial
376 base growth in Crouzon syndrome. Delivery of recombinant TNAP also decreased the incidence
377 of class III malocclusion in the C57BL/6 but not BALB/c FGFR2$^{C342Y/+}$ mice. The malocclusion
378 rescue is likely due to changes in coronal suture fusion as opposed to changes in the cranial
379 base, as treatment with TNAP had minimal and similar changes on cranial base synchondroses
380 and cranial base bone lengths in both C57BL/6 and BALB/c FGFR2$^{C342Y/+}$ mice, with an effect on
381 coronal suture fusion only in C57BL/6 FGFR2$^{C342Y/+}$ mice.
382 A major limitation of this study is the method and timing of TNAP delivery. Lentiviral
383 delivery of TNAP was not ideal, as the control group did not receive lentivirus which can lead to
384 liver toxicity and increase serum AP levels. While we found that delivery of the TNAP lentivirus
385 decreased serum ALT and increased serum AST levels in the treated mice, there was no impact
386 on body weight of the mice. We interpret these findings to indicate that the treatment had
387 minimal significant impact on overall health of the mice. In addition, serum AP levels did not
388 correlate with serum AST levels and had a reverse correlation with serum ALT levels in treated
389 FGFR2$^{C342Y/+}$ mice. We interpret this latter data to indicate that while changes in the liver may
390 have occurred, liver toxicity was not the cause for increased serum AP levels in the treated
391 mice. Yet, we cannot be certain that the lentiviral vector itself had no impact on the craniofacial
392 skeletal phenotype of the treated FGFR2$^{C342Y/+}$ mice. A more ideal study design would
393 incorporate empty lentiviral vector delivery to the control mice, or delivery of a recombinant

394 TNAP protein to the mice. It would also be worthwhile to attempt prenatal delivery of TNAP, to
395 determine if earlier treatment would have a greater impact on rescue of coronal suture fusion
396 in C57BL/6 FGFR2$^{C342Y/+}$ mice.

397 Finally, it is also worth noting that earlier time points to assess changes in the coronal
398 suture were not performed. The decreased incidence of coronal suture obliteration in C57BL/6
399 Crouzon mice at 3 weeks postnatal suggests that onset occurred later in these mice. Earlier
400 time points assessing the coronal suture after treatment could have confirmed that this was
401 indeed the case. Earlier onset of craniosynostosis increases morbidity, as brain growth is limited
402 earlier and for a longer duration. If TNAP postpones fusion of the coronal suture in Crouzon
403 syndrome, treatment with TNAP could potentially diminish morbidity.

404

405 Acknowledgments

406 We thank Prof. José Luis Millán (La Jolla, CA) and Prof. Takashi Shimada (Tokyo, Japan) for
407 providing us with the lentiviral vector expressing mineral targeted TNAP, as reported in
408 Yamamoto et al., 2011 (30).

409

410 References

411 1. Flapper WJ, Anderson PJ, Roberts RM, David DJ. Intellectual outcomes following protocol
412 management in Crouzon, Pfeiffer, and Muenke syndromes. J Craniofac Surg. 2009;20(4):1252-5.
413 Epub 2009/07/25. doi: 10.1097/SCS.0b013e3181acdf9a. PubMed PMID: 19625842.
414 2. McCarthy JG, Warren SM, Bernstein J, Burnett W, Cunningham ML, Edmond JC, et al.
415 Parameters of care for craniosynostosis. Cleft Palate Craniofac J. 2012;49 Suppl:1S-24S. Epub
416 2011/08/19. doi: 10.1597/11-138. PubMed PMID: 21848431.

417 3. Morriss-Kay GM, Wilkie AO. Growth of the normal skull vault and its alteration in
418 craniosynostosis: insights from human genetics and experimental studies. J Anat.
419 2005;207(5):637-53. Epub 2005/11/30. doi: 10.1111/j.1469-7580.2005.00475.x. PubMed PMID:
420 16313397; PubMed Central PMCID: PMCPMC1571561.
421 4. Okajima K, Robinson LK, Hart MA, Abuelo DN, Cowan LS, Hasegawa T, et al. Ocular anterior
422 chamber dysgenesis in craniosynostosis syndromes with a fibroblast growth factor receptor 2
423 mutation. Am J Med Genet. 1999;85(2):160-70. Epub 1999/07/16. PubMed PMID: 10406670.
424 5. Rasmussen SA, Yazdy MM, Frias JL, Honein MA. Priorities for public health research on
425 craniosynostosis: summary and recommendations from a Centers for Disease Control and
426 Prevention-sponsored meeting. Am J Med Genet A. 2008;146A(2):149-58. Epub 2007/12/15.
427 doi: 10.1002/ajmg.a.32106. PubMed PMID: 18080327.
428 6. Seruya M, Oh AK, Boyajian MJ, Posnick JC, Keating RF. Treatment for delayed presentation
429 of sagittal synostosis: challenges pertaining to occult intracranial hypertension. J Neurosurg
430 Pediatr. 2011;8(1):40-8. Epub 2011/07/05. doi: 10.3171/2011.4.PEDS1160. PubMed PMID:
431 21721888.
432 7. Abe H, Ikota T, Akino M, Kitami K, Tsuru M. Functional prognosis of surgical treatment of
433 craniosynostosis. Childs Nerv Syst. 1985;1(1):53-61. Epub 1985/01/01. PubMed PMID: 3986842.
434 8. Baird LC, Gonda D, Cohen SR, Evers LH, LeFloch N, Levy ML, et al. Craniofacial reconstruction
435 as a treatment for elevated intracranial pressure. Childs Nerv Syst. 2012;28(3):411-8. Epub
436 2011/11/10. doi: 10.1007/s00381-011-1615-6. PubMed PMID: 22068642.
437 9. Renier D, Lajeunie E, Arnaud E, Marchac D. Management of craniosynostoses. Childs Nerv
438 Syst. 2000;16(10-11):645-58. Epub 2001/01/11. doi: 10.1007/s003810000320. PubMed PMID:
439 11151714.
440 10. Chen L, Li D, Li C, Engel A, Deng CX. A Ser252Trp [corrected] substitution in mouse fibroblast
441 growth factor receptor 2 (Fgfr2) results in craniosynostosis. Bone. 2003;33(2):169-78. Epub
442 2003/09/23. PubMed PMID: 14499350.
443 11. Eswarakumar VP, Horowitz MC, Locklin R, Morriss-Kay GM, Lonai P. A gain-of-function
444 mutation of Fgfr2c demonstrates the roles of this receptor variant in osteogenesis. Proc Natl
445 Acad Sci U S A. 2004;101(34):12555-60. Epub 2004/08/19. doi: 10.1073/pnas.0405031101.
446 PubMed PMID: 15316116; PubMed Central PMCID: PMCPMC515096.
447 12. Reardon W, Winter RM, Rutland P, Pulleyn LJ, Jones BM, Malcolm S. Mutations in the
448 fibroblast growth factor receptor 2 gene cause Crouzon syndrome. Nat Genet. 1994;8(1):98-
449 103. Epub 1994/09/01. doi: 10.1038/ng0994-98. PubMed PMID: 7987400.
450 13. Wilkie AO, Slaney SF, Oldridge M, Poole MD, Ashworth GJ, Hockley AD, et al. Apert
451 syndrome results from localized mutations of FGFR2 and is allelic with Crouzon syndrome. Nat
452 Genet. 1995;9(2):165-72. Epub 1995/02/01. doi: 10.1038/ng0295-165. PubMed PMID:
453 7719344.
454 14. Whyte MP, Greenberg CR, Salman NJ, Bober MB, McAlister WH, Wenkert D, et al. Enzyme-
455 replacement therapy in life-threatening hypophosphatasia. N Engl J Med. 2012;366(10):904-13.
456 Epub 2012/03/09. doi: 10.1056/NEJMoa1106173. PubMed PMID: 22397652.
457 15. Collmann H, Mornet E, Gattenlohner S, Beck C, Girschick H. Neurosurgical aspects of
458 childhood hypophosphatasia. Childs Nerv Syst. 2009;25(2):217-23. Epub 2008/09/05. doi:
459 10.1007/s00381-008-0708-3. PubMed PMID: 18769927.

460 16. Fraser D. Hypophosphatasia. Am J Med. 1957;22(5):730-46. Epub 1957/05/01. PubMed
461 PMID: 13410963.
462 17. Liu J, Nam HK, Campbell C, Gasque KC, Millan JL, Hatch NE. Tissue-nonspecific alkaline
463 phosphatase deficiency causes abnormal craniofacial bone development in the Alpl(-/-) mouse
464 model of infantile hypophosphatasia. Bone. 2014;67:81-94. Epub 2014/07/12. doi:
465 10.1016/j.bone.2014.06.040. PubMed PMID: 25014884; PubMed Central PMCID:
466 PMCPMC4149826.
467 18. Galvin BD, Hart KC, Meyer AN, Webster MK, Donoghue DJ. Constitutive receptor activation
468 by Crouzon syndrome mutations in fibroblast growth factor receptor (FGFR)2 and FGFR2/Neu
469 chimeras. Proc Natl Acad Sci U S A. 1996;93(15):7894-9. Epub 1996/07/23. PubMed PMID:
470 8755573; PubMed Central PMCID: PMCPMC38845.
471 19. Neilson KM, Friesel RE. Constitutive activation of fibroblast growth factor receptor-2 by a
472 point mutation associated with Crouzon syndrome. J Biol Chem. 1995;270(44):26037-40. Epub
473 1995/11/03. PubMed PMID: 7592798.
474 20. Robertson SC, Meyer AN, Hart KC, Galvin BD, Webster MK, Donoghue DJ. Activating
475 mutations in the extracellular domain of the fibroblast growth factor receptor 2 function by
476 disruption of the disulfide bond in the third immunoglobulin-like domain. Proc Natl Acad Sci U S
477 A. 1998;95(8):4567-72. Epub 1998/05/16. PubMed PMID: 9539778; PubMed Central PMCID:
478 PMCPMC22530.
479 21. Pfaff MJ, Xue K, Li L, Horowitz MC, Steinbacher DM, Eswarakumar JVP. FGFR2c-mediated
480 ERK-MAPK activity regulates coronal suture development. Dev Biol. 2016;415(2):242-50. Epub
481 2016/04/02. doi: 10.1016/j.ydbio.2016.03.026. PubMed PMID: 27034231; PubMed Central
482 PMCID: PMCPMC5580088.
483 22. Hatch NE, Li Y, Franceschi RT. FGF2 stimulation of the pyrophosphate-generating enzyme,
484 PC-1, in pre-osteoblast cells is mediated by RUNX2. J Bone Miner Res. 2009;24(4):652-62. Epub
485 2008/12/04. doi: 10.1359/jbmr.081213. PubMed PMID: 19049325; PubMed Central PMCID:
486 PMCPMC2659512.
487 23. Hatch NE, Nociti F, Swanson E, Bothwell M, Somerman M. FGF2 alters expression of the
488 pyrophosphate/phosphate regulating proteins, PC-1, ANK and TNAP, in the calvarial
489 osteoblastic cell line, MC3T3E1(C4). Connect Tissue Res. 2005;46(4-5):184-92. Epub
490 2006/03/21. doi: 10.1080/03008200500237203. PubMed PMID: 16546821.
491 24. Liu J, Kwon TG, Nam HK, Hatch NE. Craniosynostosis-associated Fgfr2(C342Y) mutant bone
492 marrow stromal cells exhibit cell autonomous abnormalities in osteoblast differentiation and
493 bone formation. Biomed Res Int. 2013;2013:292506. Epub 2013/06/14. doi:
494 10.1155/2013/292506. PubMed PMID: 23762837; PubMed Central PMCID: PMCPMC3665166.
495 25. Liu J, Nam HK, Wang E, Hatch NE. Further analysis of the Crouzon mouse: effects of the
496 FGFR2(C342Y) mutation are cranial bone-dependent. Calcif Tissue Int. 2013;92(5):451-66. Epub
497 2013/01/30. doi: 10.1007/s00223-013-9701-2. PubMed PMID: 23358860; PubMed Central
498 PMCID: PMCPMC3631296.
499 26. Nam HK, Sharma M, Liu J, Hatch NE. Tissue Nonspecific Alkaline Phosphatase (TNAP)
500 Regulates Cranial Base Growth and Synchondrosis Maturation. Front Physiol. 2017;8:161. Epub
501 2017/04/06. doi: 10.3389/fphys.2017.00161. PubMed PMID: 28377728; PubMed Central
502 PMCID: PMCPMC5359511.

503 27. Wang E, Nam HK, Liu J, Hatch NE. The effects of tissue-non-specific alkaline phosphatase
504 gene therapy on craniosynostosis and craniofacial morphology in the FGFR2C342Y/+ mouse
505 model of Crouzon craniosynostosis. Orthod Craniofac Res. 2015;18 Suppl 1:196-206. Epub
506 2015/04/14. doi: 10.1111/ocr.12080. PubMed PMID: 25865549; PubMed Central PMCID:
507 PMCPMC4396711.
508 28. Hanawa H, Yamamoto M, Zhao H, Shimada T, Persons DA. Optimized lentiviral vector design
509 improves titer and transgene expression of vectors containing the chicken beta-globin locus
510 HS4 insulator element. Mol Ther. 2009;17(4):667-74. Epub 2009/02/19. doi:
511 10.1038/mt.2009.1. PubMed PMID: 19223867; PubMed Central PMCID: PMCPMC2835111.
512 29. Nishioka T, Tomatsu S, Gutierrez MA, Miyamoto K, Trandafirescu GG, Lopez PL, et al.
513 Enhancement of drug delivery to bone: characterization of human tissue-nonspecific alkaline
514 phosphatase tagged with an acidic oligopeptide. Mol Genet Metab. 2006;88(3):244-55. Epub
515 2006/04/18. doi: 10.1016/j.ymgme.2006.02.012. PubMed PMID: 16616566; PubMed Central
516 PMCID: PMCPMC2587042.
517 30. Yamamoto S, Orimo H, Matsumoto T, Iijima O, Narisawa S, Maeda T, et al. Prolonged
518 survival and phenotypic correction of Akp2(-/-) hypophosphatasia mice by lentiviral gene
519 therapy. J Bone Miner Res. 2011;26(1):135-42. Epub 2010/08/06. doi: 10.1002/jbmr.201.
520 PubMed PMID: 20687159; PubMed Central PMCID: PMCPMC3179312.
521 31. Millan JL, Narisawa S, Lemire I, Loisel TP, Boileau G, Leonard P, et al. Enzyme replacement
522 therapy for murine hypophosphatasia. J Bone Miner Res. 2008;23(6):777-87. Epub 2007/12/19.
523 doi: 10.1359/jbmr.071213. PubMed PMID: 18086009; PubMed Central PMCID:
524 PMCPMC2652241.
525 32. Yadav MC, Lemire I, Leonard P, Boileau G, Blond L, Beliveau M, et al. Dose response of
526 bone-targeted enzyme replacement for murine hypophosphatasia. Bone. 2011;49(2):250-6.
527 Epub 2011/04/05. doi: 10.1016/j.bone.2011.03.770. PubMed PMID: 21458605; PubMed Central
528 PMCID: PMCPMC3117961.
529 33. Liu J, Campbell C, Nam HK, Caron A, Yadav MC, Millan JL, et al. Enzyme replacement for
530 craniofacial skeletal defects and craniosynostosis in murine hypophosphatasia. Bone.
531 2015;78:203-11. Epub 2015/05/12. doi: 10.1016/j.bone.2015.05.005. PubMed PMID:
532 25959417; PubMed Central PMCID: PMCPMC4466206.
533 34. Meganck JA, Kozloff KM, Thornton MM, Broski SM, Goldstein SA. Beam hardening artifacts
534 in micro-computed tomography scanning can be reduced by X-ray beam filtration and the
535 resulting images can be used to accurately measure BMD. Bone. 2009;45(6):1104-16. Epub
536 2009/08/05. doi: 10.1016/j.bone.2009.07.078. PubMed PMID: 19651256; PubMed Central
537 PMCID: PMCPMC2783193.
538 35. Umoh JU, Sampaio AV, Welch I, Pitelka V, Goldberg HA, Underhill TM, et al. In vivo micro-CT
539 analysis of bone remodeling in a rat calvarial defect model. Phys Med Biol. 2009;54(7):2147-61.
540 Epub 2009/03/17. doi: 10.1088/0031-9155/54/7/020. PubMed PMID: 19287088.
541 36. Perlyn CA, DeLeon VB, Babbs C, Govier D, Burell L, Darvann T, et al. The craniofacial
542 phenotype of the Crouzon mouse: analysis of a model for syndromic craniosynostosis using
543 three-dimensional MicroCT. Cleft Palate Craniofac J. 2006;43(6):740-8. Epub 2006/11/16. doi:
544 10.1597/05-212. PubMed PMID: 17105336.
545 37. Richtsmeier JT, Baxter LL, Reeves RH. Parallels of craniofacial maldevelopment in Down
546 syndrome and Ts65Dn mice. Dev Dyn. 2000;217(2):137-45. Epub 2000/03/08. doi:

547 10.1002/(SICI)1097-0177(200002)217:2<137::AID-DVDY1>3.0.CO;2-N. PubMed PMID:
548 10706138.
549 38. Franca RF, Zucoloto S, da Fonseca BA. A BALB/c mouse model shows that liver involvement
550 in dengue disease is immune-mediated. Exp Mol Pathol. 2010;89(3):321-6. Epub 2010/08/03.
551 doi: 10.1016/j.yexmp.2010.07.007. PubMed PMID: 20673760.
552 39. Huang F, Zhang W, Gong G, Yuan C, Yan Y, Yang S, et al. Experimental infection of Balb/c
553 nude mice with Hepatitis E virus. BMC Infect Dis. 2009;9:93. Epub 2009/06/16. doi:
554 10.1186/1471-2334-9-93. PubMed PMID: 19523236; PubMed Central PMCID:
555 PMCPMC2717970.
556 40. Whyte MP, Simmons JH, Moseley S, Fujita KP, Bishop N, Salman NJ, et al. Asfotase alfa for
557 infants and young children with hypophosphatasia: 7 year outcomes of a single-arm, open-
558 label, phase 2 extension trial. Lancet Diabetes Endocrinol. 2018. Epub 2018/12/19. doi:
559 10.1016/S2213-8587(18)30307-3. PubMed PMID: 30558909.
560 41. Murshed M, Harmey D, Millan JL, McKee MD, Karsenty G. Unique coexpression in
561 osteoblasts of broadly expressed genes accounts for the spatial restriction of ECM
562 mineralization to bone. Genes Dev. 2005;19(9):1093-104. Epub 2005/04/19. doi:
563 10.1101/gad.1276205. PubMed PMID: 15833911; PubMed Central PMCID: PMCPMC1091743.
564 42. Nam HK, Vesela I, Siismets E, Hatch NE. Tissue nonspecific alkaline phosphatase promotes
565 calvarial progenitor cell cycle progression and cytokinesis via Erk1,2. Bone. 2018;120:125-36.
566 Epub 2018/10/21. doi: 10.1016/j.bone.2018.10.013. PubMed PMID: 30342227.
567

568 **Figure Legends:**

569

570 **Figure 1. Neonatal Coronal Suture Fusion in C57BL/6 FGFR2$^{C342Y/+}$ Mice.** Representative images

571 of dissected FGFR2$^{+/+}$ (A) and FGFR2$^{C342Y/+}$ (B) day three mouse skulls are shown. Arrows point

572 to loss of the coronal suture in C57BL/6 FGFR2$^{C342Y/+}$ mice.

573

574 **Figure 2. Body Weight and Length of BALB/c and C57BL/6 Mice.** Body weight and length of

575 vehicle vs. TNAP treated mice are shown. FGFR2$^{C342Y/+}$ mice are lighter and smaller than

576 FGFR2$^{+/+}$ mice, regardless of strain. Treatment does not alter body weight or body length.

577 *$p<0.01$ between genotypes.

578

579 **Figure 3. Micro CT Images of Vehicle and TNAP Treated FGFR2$^{C342Y/+}$ Mice.** Micro CT isosurface
580 axial images of day 28 BALB/c and day 21 C57BL/6 mouse skulls are shown. Denser bone tissues
581 are lighter in color. Comparison of BALB/c FGFR2$^{+/+}$ (WT) mice (A), BALB/c FGFR2$^{C342Y/+}$ (CZ)
582 vehicle treated mice (C), and BALB/c FGFR2$^{C342Y/+}$ (CZ) TNAP treated mice (E) indicates
583 morphologic differences between genotypes but not treatment groups. Comparison of C57BL/6
584 FGFR2$^{+/+}$ (WT) mice (B), C57BL/6 /c FGFR2$^{C342Y/+}$ (CZ) vehicle treated mice (D), and C57BL/6
585 FGFR2$^{C342Y/+}$ (CZ) TNAP treated mice (F) indicates morphologic differences between genotypes
586 but not treatment groups.
587
588 **Figure 4. Coronal Suture Fusion in Vehicle and TNAP Treated FGFR2$^{C342Y/+}$ Mice.** Percentage of
589 mice with fusion of the coronal suture are shown. Fusion was scored in the following
590 categories: 0) normal open suture, 1) diminished suture width with no fusion, 2) diminished
591 suture width with point fusions across the suture, and 3) obliteration of the suture. Results
592 show diminished suture obliteration in C57BL/6 FGFR2$^{C342Y/+}$ (Crouzon) mice with no changes
593 noted in BALB/c FGFR2$^{C342Y/+}$ (Crouzon) mice. *$p<0.03$ between treatment groups.
594
595 **Figure 5. Incidence of Malocclusion in Vehicle and TNAP Treated FGFR2$^{C342Y/+}$ Mice.**
596 Percentage of FGFR2$^{C342Y/+}$ (Crouzon) mice with a class III malocclusion are shown. Treatment
597 with TNAP lentivirus significantly diminished malocclusion in C57BL/6 FGFR2$^{C342Y/+}$ (Crouzon)
598 but not BALB/c FGFR2$^{C342Y/+}$ (Crouzon) mice. *$p<0.03$.
599

600 **Figure 6. Liver Toxicity Enzyme Tests in Vehicle and TNAP Treated FGFR2$^{C342Y/+}$ Mice.** Alanine
601 amino transferase (ALT) and aspartate amino transferase (AST) liver enzymes were measured in
602 serum of vehicle and treated mice. When compared by groups, no differences were seen
603 between FGFR2$^{+/+}$ and FGFR2$^{C342Y/+}$ vehicle treated mice. Treatment decreased serum ALT (A)
604 and increased serum AST (B) in FGFR2$^{C342Y/+}$ mice. Linear regression analyses showed a
605 significant reverse correlation ($r = -.73$; 95% CI of -.898 to -.361, $p < .005$) between AP and ALT
606 enzyme levels in FGFR2$^{C342Y/+}$ mice (C). No correlation was found between AP and AST enzyme
607 levels in FGFR2$^{C342Y/+}$ mice (D). No correlations were found between ALT (E) or AST (F) enzyme
608 levels and body weight.

FIGURES

Fig. 1. Neonatal Suture Fusion in C57BL/6 Crouzon Mice.

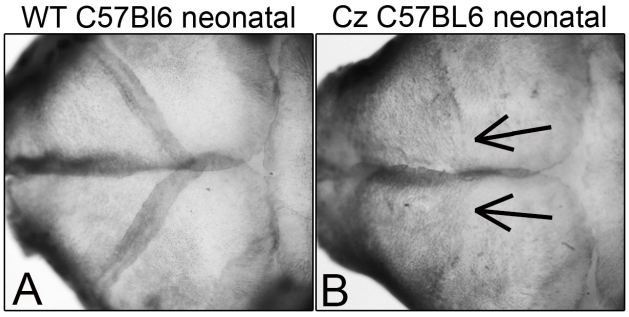

Fig. 2. Body Weight and Length of BALB/c and C57BL/6 Mice.

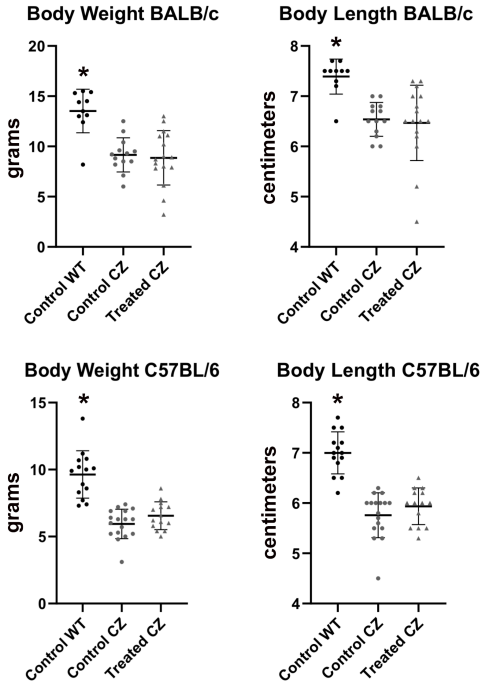

Fig. 3. Isosurface Images of BALB/c and C57BL/6 Mice.

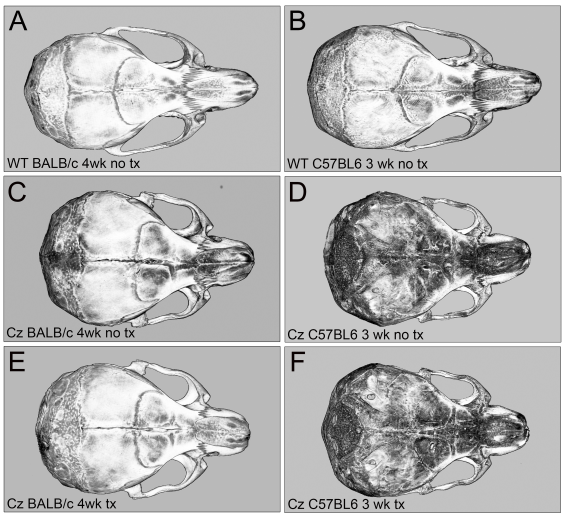

Fig. 4 Coronal Suture Fusion in BALB/c and C57BL/6 Mice.

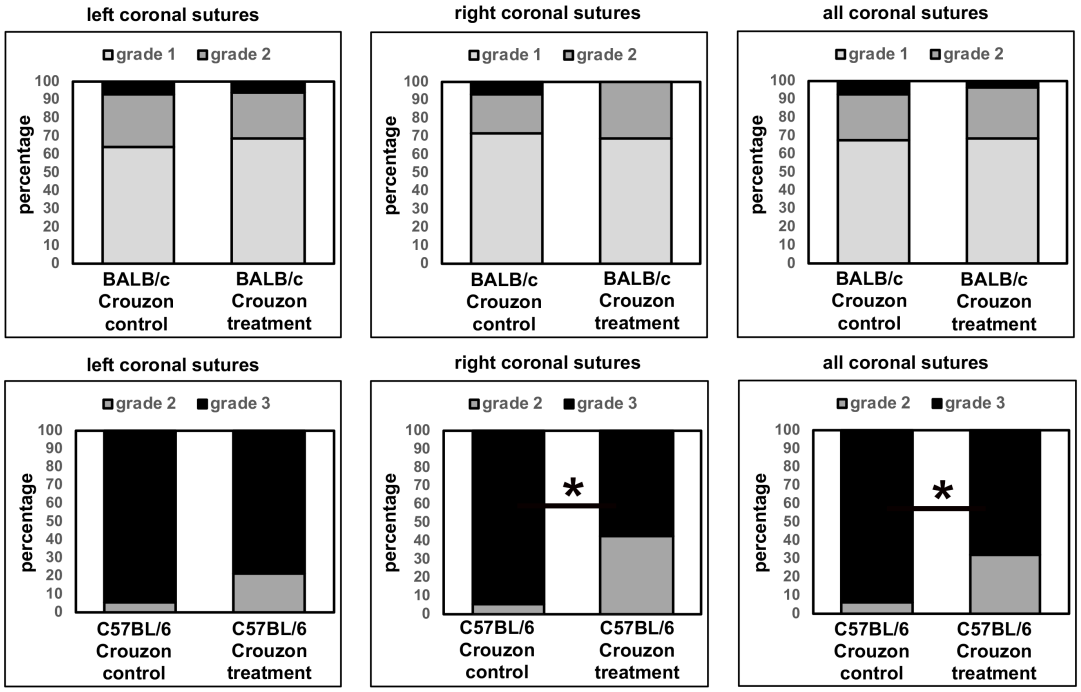

Fig. 5. Class III Malocclusion in BALB/c and C57BL/6 Mice.

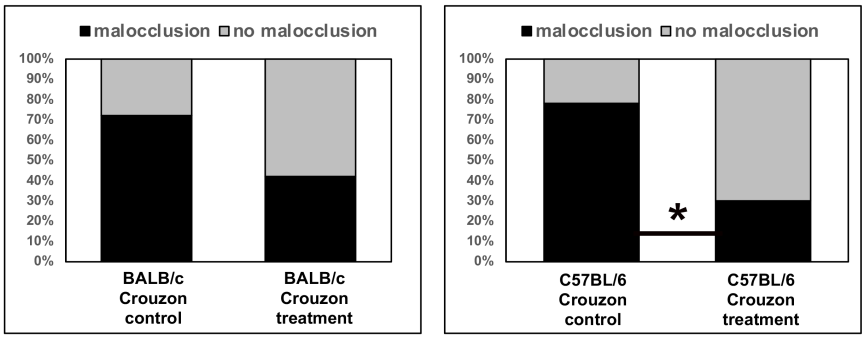
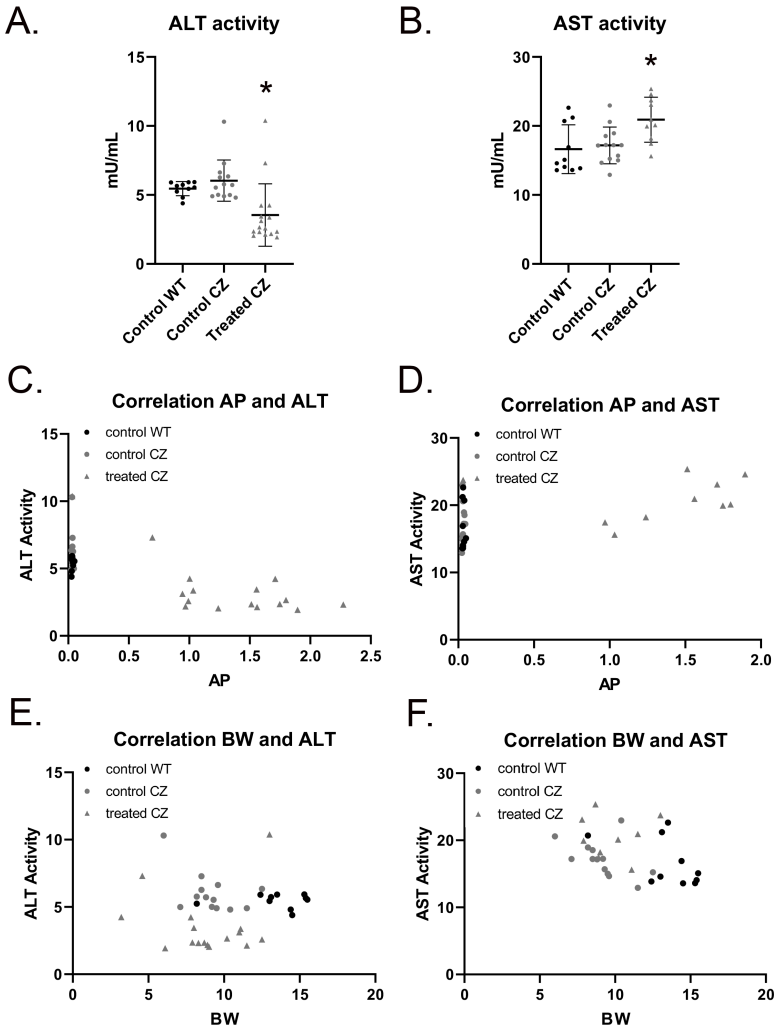
Fig. 6. Liver Enzyme Tests in Control and Treated Mice